Title

The Impact of Carbonate Texture on the Quantification of Total Porosity by Image Analysis

Authors and Addresses

Thomas J. Haines[1,2]

Joyce E. Neilson[1]

David Healy[1]

Emma A. H. Michie[1,3]

Andrew C. Aplin[4]

[1] School of Geosciences, King's College, University of Aberdeen, Aberdeen AB24 3UE, UK

[2] Badley Ashton and Associates Ltd, Winceby House, Winceby, Horncastle, Lincolnshire LN9 6PB, UK

[3] Badley Geoscience Ltd, North Beck House, North Beck Lane, Hundleby, Lincolnshire PE23 5NB, UK

[4] Dept. of Earth Sciences, Durham University, Durham DH1 3LE, UK

Corresponding author

Thomas J. Haines,

Email: tj.haines.88@gmail.com

Telephone: +447917692228,

Correspondence/ present address: Badley Ashton and Associates Ltd, Winceby House, Winceby, Horncastle, Lincolnshire LN9 6PB, UK

Abstract

Image analysis is widely used to quantify porosity because, in addition to porosity, it can provide quantitative pore system information, such as pore sizes and shapes. Despite its wide use, no standard image analysis workflow exists. When employing image analysis, a workflow must be developed and evaluated to understand the methodological pitfalls and assumptions to enable accurate quantification of total porosity. This study presents an image analysis workflow that is used to quantify total porosity in a range of carbonate lithofacies. This study uses stitched BSE-SEM photomicrographs to construct greyscale pore system images, which are systematically thresholded to produce binary images composed of a pore phase and a rock phase. The ratio of the area of the pore phase to the total area of the pore system image defines the total porosity. Image analysis total porosity is compared with total porosity quantified by standard porosimetry techniques (He-porosimetry and Mercury injection capillary pressure (MICP) porosimetry) to understand the systematics of the workflow. The impact of carbonate textures on image analysis porosity quantification is also assessed.

A comparison between image analysis, He-porosimetry and MICP total porosity indicates that the image analysis workflow used in this study can accurately quantify or underestimate total porosity depending on the lithofacies textures and pore systems. The porosity of wackestone lithofacies tends to be significantly underestimated (i.e. greater than 10 %) by image analysis, whereas packstone, grainstone, rudstone and floatstone lithofacies tend to be accurately estimated or slightly underestimated (i.e. 5 % or less) by image analysis. The underestimation of image analysis porosity in the wackestone lithofacies is correlated to the quantity of matrix pore types and is thought to be caused by incomplete imaging of micro porosity and by non-representative field of views. Image analysis porosity, which is calculated from 2D areas, is comparable with 3D porosity volumes in lithofacies that lack or

are weakly microporous; in such lithofacies, image analysis is assumed to be accurately measuring other 2D parameters, including pore sizes and shapes.

Keywords

image analysis; porosity quantification; carbonates; lithofacies

Text

1 Introduction

Porosity is one of the key measurements used to understand the physical properties of rocks, e.g. permeability, acoustic velocity and mechanical strength. Porosity can be characterised by a range of different methodologies including He-porosimetry, Mercury injection capillary pressure (MICP) analysis, point count analysis and image analysis. Porosimetry methodologies, which derive porosity by quantifying the grain and bulk densities or volumes, may fail to quantify porosity that is unconnected to the pore system and therefore can underestimate porosity (Galaup et al., 2012). Point count analysis quantifies porosity by counting the number of pores in a thin section. This methodology is associated with large errors of up to 100 % (Halley, 1978), which are related to the incorrect assumption that the area of porosity on a 2D thin section is proportional to the 3D pore volume and the underrepresentation of submicroscopic porosity (Halley, 1978).

Image analysis methodologies convert photomicrographs of thin sections into two binary phases: 1) the rock phase and 2) the pore phase (Ehrlich et al., 1991). Image analysis total porosity is defined as the ratio of the pore phase area to the bulk area of a rock and is commonly given as a percentage (Anselmetti et al., 1998). Image analysis can suffer from the same problems as point counting. The accuracy of image analysis is limited by the quality of photomicrographs and by operator error in dividing the photomicrograph into the rock and pore phases (Andriani and Walsh, 2002; Grove and Jerram, 2011). However, image analysis has a key advantage over the other porosity quantification methodologies; it provides valuable quantitative information on the pore system characteristics of a rock, e.g. pore types, sizes and shapes (e.g. Berrezueta et al., 2015).

Modal abundances of porosity and pore system characteristics can also be measured directly in three dimensions using X-ray CT scanners (Wildenschild and Sheppard, 2013). Although limited by sample size, the resolution of such X-ray CT measurements can be as low as a few microns, (Jerram and Higgins, 2007) and is improving all the time (Wildenschild and Sheppard, 2013). However, this technique requires expensive equipment and significant processing time (Jerram and Higgins, 2007). Conversely, image analysis does not require specialist equipment and can be processed relatively quickly (Berrezueta et al., 2015; Grove and Jerram, 2011). It has the potential to provide quick, accurate and reproducible analysis of rock properties with limited user bias (Grove and Jerram, 2011). Accordingly, image analysis is widely used to quantify porosity and pore system characteristics, particularly in carbonate lithologies (e.g. Anselmetti et al., 1998; Weger et al., 2009).Despite its wide use, no standard image analysis workflow exists. For example, Anselmetti et al. (1998) acquire optical photomicrographs to analyse macro porosity and ESEM photomicrographs to analyse micro porosity. Conversely, Weger et al. (2009) use optical photomicrographs under extinction in cross polarised light to image and segment porosity. To accurately quantify porosity using image analysis techniques, a systematic workflow must be developed and evaluated to understand the methodological pitfalls and assumptions.

This study outlines the development of an image analysis workflow that uses backscatter SEM images to quantify porosity in a range of carbonate lithofacies. To provide an understanding of the systematics of the image analysis workflow, including how carbonate textures impact porosity quantification by image analysis, porosity is also quantified by standard porosimetry techniques (helium and mercury) in the same carbonate lithofacies. The research ultimately provides a detailed understanding of the methodological pitfalls and assumptions of image analysis, which are essential to accurately quantify porosity and understand the physical properties of rocks.

2 Sample Database

A database of 31 rock samples was collected from outcrop exposures of the Oligo-Miocene stratigraphy on the Maltese Islands to evaluate the pitfalls and assumptions of total porosity quantification by image analysis.

The stratigraphy of the Maltese Islands is subdivided into four Formations (Pedley et al., 1976), however, this study focusses on the lowermost two exposed Formations: the Oligocene Lower Coralline Limestone Formation and the Miocene Globigerina Limestone Formation. The Lower Coralline Limestone Formation is subdivided into four Members, which are, in stratigraphic order: 1) Il Maghlaq, 2) Attard, 3) Xlendi and 4) Il Mara Members (Pedley, 1978). The Lower Coralline Limestone Formation is dominantly composed of coralline algae and larger benthic foraminifera rich wacke-, pack-, grain-, float- and rudstones (Figure 1 a and b) (Healy et al., 2014; Michie et al., 2014). The Globigerina Limestone Formation is subdivided into three members (Pedley et al., 1976), which are separated by hardground-conglomerate couplets. The three Members are, in stratigraphic order: 1) Lower Globigerina, 2) Middle Globigerina and 3) Upper Globigerina Limestone Members (Pedley et al., 1976). This Formation is composed of bryozoa wacke- and packstones and planktonic foraminiferal lime mudstones and wackestones (Figure 1 c and d) (Healy et al., 2014; Michie et al., 2014). Table 1 summarises the lithofacies classification of the Oligo-Miocene stratigraphy on the Maltese Islands used in this study.

The 31 samples in the sample database included packstones, pack-/ grainstones, rudstones and floatstones from Lower Coralline Limestone Formation (Figure 1 a and b) and wackestones from the Globigerina Limestone Formation (Figure 1 c and d) (Table 1).

3 Methodology

3.1 Helium Porosimetry

84 1 inch (25.4 mm) diameter core plugs were prepared from the 31 samples in the sample database. Multiple core plugs were cut from the same rock sample where possible to measure porosity heterogeneity on the core plug scale. A Coberly-Stevens porosimeter was used to quantify the He-porosity on the 84 core plugs at ambient temperature and pressure conditions.

3.1.1 Total Porosity Calculation

He-porosity was calculated from the bulk volume, V_b, and the grain volume, V_g, of the core plug as follows (Equation 1)

Equation 1 $$He\ \phi\ (\%) = \frac{V_b - V_g}{V_g} \times 100$$

The measurement of He-porosity was repeated three times for each core plug to reduce experimental error. The He-porosity value quoted in this study is the arithmetic mean of the three porosity measurements for every core plug in each rock sample.

3.2 Image Analysis

Thin section image analysis was used to quantify porosity in all 31 samples in the sample database.

3.2.1 Thin Section Preparation

Each of the 31 rock samples were cut into 3 perpendicular planes, from which, 3 thin sections (x, y and z) were prepared (93 thin sections in total). The thin sections were cut in close proximity to the corresponding sample core plugs to enable direct comparisons between image analysis and He-porosimetry datasets.

3.2.2 Image Acquisition

In quantifying pore system characteristics, various authors have used images acquired by different microscopy techniques, such as optical microscopy and scanning electron microscopy, to conduct image analysis (Anselmetti et al., 1998; Berrezueta et al., 2015; Grove and Jerram, 2011; Hollis et al., 2010; Lønøy, 2006; Rustichelli et al., 2013; Weger et al., 2009).

The use of optical microscopy in image analysis is commonly reliant upon the impregnation of pore space by blue dyed epoxy resin (Grove and Jerram, 2011) (Figure 2). However, the impregnation of pore space by blue dyed epoxy resin is a process that requires care and attention because in some instances it can incompletely impregnate the porosity.Figure 2 provides an example taken from the sample database of this study where the blue dyed epoxy resin has incompletely filled the pore system and as a result poorly defines the porosity. A photomicrograph of the same field of view taken in back-scatted electron mode on a scanning electron microscope (BSE-SEM) is also provided and appears to define the pore spaces more accurately (Figure 2 c). In this study, pore system images were acquired using BSE-SEM to avoid any porosity quantification errors that may have resulted from the incomplete filling of pores by blue dyed epoxy resin.

Pore system images were systematically acquired using BSE-SEM, which produces greyscale images (Figure 3 b). When using greyscale images in image analysis, a common problem is the lack of contrast of between the phases of interest (porosity and rock) (Andriani and

Walsh, 2002; Grove and Jerram, 2011). To overcome this potential problem, each pore system image was systematically acquired with identical brightness and contrast values, which provided a significant level of contrast between the phases of interest. Additionally, the brightness and contrast values were selected and cross checked with spot energy-dispersive X-ray spectroscopy (EDS) to confirm that the image accurately represented the pore system. A systematic image acquisition workflow enabled a more precise comparison of porosity between different pore system images in the same thin section and between thin sections in the same rock sample and different rock samples.

A minimum of 6 BSE-SEM images of equal magnification were acquired and stitched together to create a pore system image (Figure 3 b and c). The stitching of images enabled the imaging of pores with diameters ranging from less than 0.5 microns to greater than 1000 microns. Three different pore system images were collected from each thin section. Pore system images were collected from the bottom, centre and top of each thin section and labelled B, C and T respectively (Figure 3 a). As a result, a minimum of 18 photomicrographs were used to quantify the porosity on each thin section, which is consistent with the quoted number of field of views required to enable representative image analysis porosity quantification (Ehrlich et al., 1991; Solymar and Fabricius, 1999).

The image acquisition workflow was repeated on perpendicularly oriented thin sections (x, y and z) in each rock sample to acquire pore system images that allowed the quantification of porosity in three dimensions (Figure 4). Consequently, the porosity of each rock sample was quantified from 9 pore system images, which were composed of a minimum of 54 individual BSE-SEM photomicrographs.

3.2.3 Image Processing

The BSE-SEM pore system images were composed of greyscale pixels (Figures 3 and 4). The pore system images were subdivided into two phases according to the greyscale values of the pixels: 1) the rock phase, which was mono- or polymineralic and was represented by any greyscale value except those that represent black and 2) the pore phase, which was represented by black greyscale values. The image acquisition approach, outlined above, allowed for minimal image processing, which was limited to systematic greyscale thresholding of the BSE-SEM images. The thresholding process replaced all greyscale values associated with the rock phase to create a binary image, in which, the white corresponded to the rock phase and black corresponded to the pore phase (Figure 4 e).

3.2.4 Total Porosity Calculation

Each pixel in a pore system image represented an area, the exact dimensions (in μm^2) of which, were defined by the magnification of the original image. ImageJ 1.48i was used to quantify the area of pixels that represented the pore system, i.e. black pixels (0) (Rasband, 2014). The porosity of individual pore system images was calculated as the ratio of the total area of black pixels to the total area of pixels (equation 2). The image analysis porosity of a thin section was calculated as the arithmetic mean of the porosity values calculated from the corresponding B, C and T pore system images (equation 3). The image analysis porosity of a rock sample was calculated as the arithmetic mean of the porosity values calculated from each pore system image on the corresponding x-, y- and z-thin sections (equation 4). The image analysis porosity of a rock sample is termed the *mean image analysis porosity*.

Equation 2 $$\textit{Pore system image } \phi\,(\%) = \frac{\text{total area of black pixels}}{\text{total area of pixels}} \times 100$$

Equation 3 $$\textit{Thin section } \phi\,(\%) = \frac{\text{pore system image } \phi \text{ of } (B + C + T)}{3}$$

Equation 4 $$\textit{Mean image analysis porosity } \phi\ (\%) = \frac{\text{pore system image } \phi \text{ of } (B + C + T) \text{ of x−,y−and z−thin sections}}{9}$$

3.3 Mercury Injection Capillary Pressure (MICP) Analysis

MICP analyses were used to quantify total porosity in 23 out of the 31 samples in the sample database. MICP analyses were not conducted on the complete sample database due to experimental restrictions.

3.3.1 Sample Preparation

The 23 samples were cut from an area which represented the bulk rock and that was in close proximity to corresponding thin sections and core plugs to enable direct comparisons between the He-porosimetry and image analysis datasets.

3.3.2 Total Porosity Calculation

The Hg-porosity (pore volume) derived from MICP analyses was calculated as the ratio of dry bulk density to grain density (equation 5, 6 and 7).

Equation 5 $$V_s = V_t - V_{Hg}$$

Equation 6 $$\rho_d\ (g/cm^3) = \frac{m_s}{V_s}$$

Equation 7 $$Hg\ \phi\ (\%) = (1 - \frac{\rho_d}{\rho_g}) \times 100$$

The total sample volume, V_s, was derived from the volume of mercury, V_{Hg}, and the total volume, V_t (equation 5). The dry bulk density, ρ_d, of the sample was calculated from the sample mass, m_s, and total sample volume, V_s (equation 6). The Hg-porosity, $Hg\ \phi$, was calculated as the ratio of dry bulk density, ρ_d, to the grain density, ρ_g, (equation 7), which is 2.71 g/cm^3 for a rock composed purely of calcite.

3.4 Point Count Analysis

Point count analysis was used to estimate the quantities of pore types in 29 samples from the sample database. The point analysis was conducted on the same thin sections in which total porosity was quantified by image analysis. Point count analyses were not conducted on the complete sample database due to experimental restrictions.

The point count methodology utilized high resolution optical full thin section photomicrographs, obtained using thin section scanning equipment, to systematically count pore types. The optical photomicrographs were fixed to equal dimensions and resolution. A square mesh of dashed lines, of equal dimensions, was centred over the top of each full thin optical photomicrograph. Every pore that intersected the mesh was counted and weighted according to the number of dashes intersecting its length. This methodology was utilized, over standard point counting methodologies, to provide a degree of repeatability to the point count data.

In the majority of instances, this methodology counted in excess of 300 points, which is in line with the quoted number of points (250 - 300) required for statistically significant results (e.g. Tucker et al., 1988; Mock and Jerram, 2005; Morgan and Jerram, 2006). In the instances where less than 300 points were counted, the porosity tended to be very low. To increase the statistical significance in such instances, multiple thin sections from the same sample were analysed. Similarly, if significant textural heterogeneity was observed between different thin sections in the same sample, multiple thin sections were analysed. Pore type data are presented as dominant pore types (Table 2); dominant pore types are defined as those with the highest occurrence in a sample.

3.4.1 Pore Type Terminology

Pore types were classified according to the porosity classification systems of Lønøy (2006) and Choquette and Pray (1970). Pore types were subdivided into eight categories according to sedimentological, diagenetic and damage textural characteristics. Pore types included intergranular, intragranular, intercrystalline, mudstone micro porosity (matrix), mouldic, vuggy, fracture and breccia (Choquette and Pray, 1970; Lønøy, 2006).

Inter- and intragranular pore types are synonymous with inter- and intraparticle pore types respectively (Choquette and Pray, 1970; Lønøy, 2006). Additionally, this study utilized the mudstone microporosity classification of Lønøy (2006). Mudstone microporosity is defined as extremely small (less than 10 μm in diameter (Lønøy, 2006)) pores of intergranular or intercrystalline type that are only discernable under the optical microscope by the infilling of the matrix by blue dyed epoxy resin (Lønøy, 2006). For the purposes of this study, mudstone micro pore types were re-named as matrix pore types to avoid confusion surrounding pore size classifications. Matrix pore types were defined as pore types which were too small to be accurately characterised by point counting techniques but were visible under optical microscopy. All other pore types definitions used in this study were identical to those of previous pore type classifications (Choquette and Pray, 1970; Lønøy, 2006).

4 Results

4.1 Image Analysis Methodological Development

4.1.1 Pore System Image Magnification

The magnification of pore system images is an important control on the porosity value quantified by image analysis (Andriani and Walsh, 2002; Ehrlich et al., 1991). Porosity calculated from image analysis changes according to increasing image magnification (Figure 5). In figure 5, the field of view of the pore system is the same in each image and the magnification is increased by from 47 times to 470 times. Image analysis porosity is quantified in each image; the porosity increases from 21.43 % at 47 times magnification to 25.66 % at 470 times magnification. This is a 4.23 % increase in absolute porosity, which equates to a 16.48 % total percentage change. The largest increase in image analysis porosity occurs when the image magnification increases above 100 times. The increase in magnification corresponds to a decrease in the area represented by 1 pixel from 3.151 to 0.032 μm^2 respectively.

Higher resolution pore system images more accurately image microscopic pores by comparison to low resolution pore system images. The image analysis porosity of rocks with pore systems composed of significant quantities of microscopic pores will be under represented at low image resolutions. Consequently, image analysis porosity, in such instances, increases with image resolution until the image resolution of the pore system image accurately represents the microscopic porosity of the rock sample. In image analysis, it is essential to quantify porosity with an image resolution that accurately captures all pore sizes. The resolution of pore system images used in this study to accurately quantify porosity is 0.157 μm^2 per pixel or less.

4.1.2 Sampled Thin Section Area

It is suggested that 15 to 30 fields of view are necessary to accurately represent the porosity in reservoir rocks (Ehrlich et al., 1991; Solymar and Fabricius, 1999). However, as shown in the previous section, the magnification of the fields of view must be considered. This study assesses the sampled thin section area required to represent porosity in different lithofacies, rather than the number of field of views (Figure 6).

The *mean image analysis porosity* for a given sample is the cumulative value quantified from 9 pore system images (see *3.2 Image Analysis*). The mean is fixed for a set of 9 pore system images, however, when less than 9 images are used in the calculation, the cumulative value varies according to the sequence in which the pore system images (and associated sampled areas) are incorporated into the calculation. To understand the impact of the sampled area on image analysis porosity, it is important to consider the sequence in which pore system images are incorporated into the cumulative mean calculation.

The variation in the cumulative mean porosity according to the cumulative thin section area analysed is quantified by incorporating the image analysis porosity value associated with each pore system image in a given sample to the cumulative mean calculation in ascending (least to most porous) and descending (most to least porous) order (Figure 6). This approach defines upper and lower bounds, which quantify the highest and lowest possible cumulative mean image analysis porosity values associated with a set of pore system images for a given sample. These bounds are compared to the 95 % confidence intervals (CI) of the *mean image analysis porosity* to quantify the area of the thin section that needs to be sampled to represent the *mean image analysis porosity* (Figure 6).

The minimum area of the thin section that must be analysed to quantify porosity representatively is estimated as the area at which the cumulative mean image analysis porosity intersects the 95 % confidence intervals (Figure 6). The minimum area varies from 0.013 cm^2 in the PFW lithofacies (wackestone) to 0.072 cm^2 in the RBP lithofacies (packstone), which equates to approximately 0.1 and 0.5 % of the total thin section areas respectively (Figure 6). The documented variation is likely to reflect pore size differences between the two lithofacies. Average pore sizes are estimated using the image analysis workflow outlined in this study (see *3.2 Image Analysis*) and are described using the Feret Diameter descriptor in ImageJ (Rasband, 2014). The PFW lithofacies has an average pore size of 24 µm, whereas the RBP lithofacies has an average pore size of 210 µm (Figure 6).

This suggests that if the pore system is composed of larger pores, a larger area is required to represent porosity.

4.2 Total Porosity

Histograms displaying the total porosity quantified by He-porosimetry (He-porosity), MICP analysis (Hg-porosity) and image analysis (*mean image analysis porosity*) methodologies are displayed in Figure 7. The total porosity distributions derived from He-porosimetry and MICP analysis methodologies are uniform and range from 1.28 to 37.25 %. For the same rock samples, the total porosity distribution derived from image analysis is normal, with a mean of 12.40 % and a range of 0.51 to 24.08 %.

4.3 Pore Types

The pore type compositions of the studied lithofacies units are displayed in Table 2 and Figure 8. The pore type compositions range from dominantly intergranular, intragranular and matrix pore types to dominantly vuggy, mouldic, fracture and breccia pore types depending upon the primary lithofacies and the diagenetic histories of the lithofacies units (Table 2 and Figure 8).

4.4 Comparison of Total Porosity According to Methodology

A comparison of porosity values derived from He-porosimetry, MICP analysis and image analysis methodologies for corresponding rock samples provides an understanding of the porosity variation according to the quantification methodology (Figure 9). An understanding of the porosity variability according to methodology is essential to accurately quantify porosity.

Figure 9 a is a cross plot of the mean He-porosity and the Hg-porosity. A coefficient of determination, R^2, of 0.929 indicates that 92.9 % of the variation in porosity according to methodology can be represented by the regression line *Hg* = -0.38 + 1.05*He* (*Hg* = Mean Hg-porosity, *y*, and *He* = He-porosity, *x*). This regression line equation is comparable to that of a 1:1 relationship between He- and Hg-porosity, i.e. a regression line expressed by the equation y = 1*x*.

Figure 9 b is a cross plot of the mean He-porosity and the *mean image analysis porosity* for each sample. The coefficient of determination, R^2, for this linear regression equation is 0.521. This indicates that 52.1 % of the variation in porosity according to methodology can be explained by the linear regression equation *IA* = 4.7 + 0.41*He* (*IA* = *Mean image analysis porosity*, *y*, and *He* = He-porosity, *x*). This equation is significantly different from that of y = 1*x*, which would indicate that the He-porosity and *mean image analysis porosity* are equal. It is therefore apparent that the porosity values quantified by image analysis are significantly different to the porosity values quantified by He-porosimetry and MICP techniques. The linear regression equation generally indicates that the estimated value of porosity derived from image analysis is less than the He-porosimetry porosity.

5 Discussion

5.1 The Underestimation of Image Analysis Porosity

Porosity values quantified by He-porosimetry and image analysis in the same rock samples can be incomparable; in the same rock sample, the *mean image analysis porosity* can be significantly less than the mean He-porosity (Figure 9 b). This indicates that the image analysis workflow used in this study underestimates porosity or that the He-porosimetry methodology overestimates porosity. Porosimetry methodologies can underestimate porosity when a pore system is composed of significant amounts of unconnected porosity (Galaup et al., 2012), however, it is unlikely that He-porosimetry is overestimating porosity because of the strong agreement in porosity values between the He-porosimetry and MICP analysis methodologies (Figure 9 a). It is therefore assumed that the image analysis methodology is underestimating porosity.

5.2 The Influence of Lithofacies and Pore Systems

The mean porosity difference ($\Delta\phi$) is defined as the mean difference in porosity between the He-porosimetry and image analysis methodologies for the same rock sample. The mean porosity difference for each rock sample is subdivided according to the primary lithofacies to assess the impact of texture on the underestimation of porosity by image analysis (Figure 10). The mean porosity difference varies according to lithofacies (Figure 10), which indicates that the texture of a rock imparts a control on the quantification of porosity by image analysis.

The Reworked Bioclastic Packstone (RBP) lithofacies has a mean porosity difference of approximately 1 % (Figure 10). The lower 95 % confidence interval of the RBP lithofacies intersects the 0 % mean porosity difference line (red line, Figure 10). This indicates that there is no significant difference between the porosity value quantified by He-porosimetry and image analysis in the RBP lithofacies, i.e. image analysis is accurately quantifying porosity.

In the other lithofacies units, the confidence intervals do not intersect the 0 % mean porosity difference line , which indicates that there is a difference between the porosity values quantified by He-porosimetry and image analysis (Figure 10). For example, in the Planktonic Foraminifera Wackestone (PFW) lithofacies, (in both the Lower (LGL) and Middle Globigerina Limestone (MGL) Members) the mean porosity difference is greater than 10 %. This suggests that image analysis is underestimating porosity by a minimum of 10 % in wackestone lithofacies. Conversely, in the Bryozoa Wackestone (BW), Coralline Algae Pack-/ Grainstone (CAP/G), Larger Benthic Foraminifera Pack-/ Rudstone (LBFP/R) and

Rhodolith Floatstone (RF) lithofacies, the mean porosity difference is approximately 5 % or less (Figure 10).

The wackestone lithofacies in this study tend to be composed of matrix pore types and to a lesser extent intragranular pore types. A comparison of the mean porosity difference and the amount of porosity composed of matrix pores types is provided to assess the impact of matrix pore types on the difference in porosity according to the He-porosimetry and image analysis methodologies (Figure 11). In lithofacies where the quantity of matrix pore types is less than 3 % total porosity, the mean porosity difference is commonly 5 % or less (Figure 11). This suggests that the image analysis methodology accurately quantifies total porosity in lithofacies lacking matrix pore types. In rock samples where the amount of matrix pore types is greater than 5 % total porosity, the mean porosity difference is commonly 10 % or greater, which indicates that the underestimation of image analysis porosity is related to matrix pore types.

5.3 Why Does Image Analysis Underestimate Porosity?

The underestimation of porosity by image analysis is commonly documented to varying degrees (Anselmetti et al., 1998; Cerepi et al., 2001; Mowers and Budd, 1996; Neto et al., 2014; Zhang et al., 2014). Mowers and Budd (1996) compare core plug porosity with image analysis porosity in two dolostone reservoir units; the results show that image analysis porosity is consistently lower than core plug porosity. The underestimation of image analysis porosity is explained by incomplete and inaccurate filling and imaging of porosity filled with blue dyed epoxy and by low image resolution which prevents the accurate imaging of microporosity (Mowers and Budd, 1996). By using high resolution, stitched, BSE-SEM images, this study eliminates porosity quantification errors associated with both the incomplete filling of pores with blue dyed epoxy and low image resolutions. These explanations of the underestimation of image analysis porosity can therefore be ruled out in this study. The underestimation of image analysis porosity is also linked to non-representative field of views and the incomplete imaging of micro porosity (Anselmetti et al., 1998; Cerepi et al., 2001; Zhang et al., 2014).

5.3.1 Is the Image Analysis Methodology Representative?

Anselmetti et al. (1998) compare image analysis porosity and He-porosity in carbonate lithologies. In the Anselmetti et al. (1998) study, the image analysis porosity is underestimated by as much as 15 % by comparison to He-porosity; the underestimation is explained by non-representative field of views (Anselmetti et al., 1998). As previously mentioned, it is suggested that 15 to 30 fields of view are required to accurately represent the porosity in reservoir rocks (Ehrlich et al., 1991; Solymar and Fabricius, 1999). This study uses 9 pore system images, each of which is composed of a minimum of 6 fields of view stitched together (i.e. 54 fields of view in total), to quantify porosity in each rock sample.

To understand if the underestimation of image analysis porosity is related to unrepresentative field of views in the pore system images, helium and image analysis porosity distributions are compared in two contrasting lithofacies (Figure 12), in which the porosities are 1) accurately quantified (RBP lithofacies) and 2) underestimated (BW lithofacies) by image analysis (see Figure 10). In the RBP lithofacies (packstone, see Table 1), in which image analysis accurately quantifies porosity, the helium and image analysis porosity distributions are similarly normal with comparable means (Figure 12 a and b). This indicates that the pore system images used to quantify porosity by image analysis in this packstone lithofacies are representative at the core plug scale. In the BW lithofacies (wackestone, see Table 1), the image analysis porosity is underestimated by greater than 5 % by comparison to the helium porosity (Figure 10). In this lithofacies, the helium and image analysis porosity distributions are incomparable (Figure 12 c and d). The helium porosity distribution is normal, which indicates that porosity can be accurately described by a mean value on the core plug scale, whereas the image analysis porosity distribution is weakly uniform to random. This suggests that the pore system images in this wackestone lithofacies are inaccurately representing the porosity and are a source of the error in image analysis porosity quantification

5.3.2 Incomplete Imaging of Micro Porosity

Cerepi et al. (2001) compare porosity values quantified from image analysis and MICP analysis in a range of carbonate textures. The image analysis workflow used in the Cerepi et al. (2001) study results in image analysis porosity values that are consistently lower than the MICP analysis derived porosity values. The difference in porosity between the two techniques is explained by poor and/ or incomplete imaging of the micro porosity by the image analysis method (Cerepi et al., 2001).

According to most definitions, micrite particles range between 1 and 10 microns in size (Deville de Periere et al., 2011). Micro pores, which are often hosted between micrite particles, are defined by Cantrell and Hagerty (1999) as pores that are 10 microns or less in size. Standard thin sections, including those used in this study, are 30 microns in thickness. A standard thin section of a micritic matrix is likely to be composed of multiple micrite particles stacked upon one another with variably abundant micro porosity hosted between individual particles (Figure 13). Photomicrographs of pore systems capture 2D images of the upper surfaces of thin sections; the photomicrographs do not capture the 3D stacking of micrite particles nor do they capture all of the micro porosity hosted between the micrite particles (Figure 13). Despite high levels of magnification, some micro porosity is hidden from the view captured in the photomicrograph and is therefore not quantified by image analysis. The ‘hidden’ porosity is likely to be a source of the underestimation of image analysis porosity in wackestone lithofacies in this study, along with non-representative field of views.

6 Summary: Methodological Implications

- Total porosity can be quantified by a range of different methodologies; each methodology has pitfalls and uncertainties. Image analysis, in addition to quantifying total porosity, can quantify pore system characteristics, such as pore sizes and shapes, and hence is a powerful tool used to characterise heterogeneous and complex pore systems in reservoir rocks. Despite this, no standard image analysis workflow exists. This study evaluates the uncertainties in an image analysis workflow, which is used to quantify porosity in a range of carbonate lithofacies.
- The image analysis workflow uses stitched BSE-SEM photomicrographs to construct pore system images. The pore system images, which are greyscale, are systematically thresholded to produce binary images that are composed of a pore phase and a rock phase. The ratio of the area of the pore phase to the total area of the pore system image defines the total porosity.
- The porosity quantified by image analysis is compared with conventional porosimetry porosities(He-porosity and MICP porosity) to understand the pitfalls and assumptions of the image analysis workflow
- He-porosimetry and MICP derived total porosity are comparable and are considered to accurately reflect the total porosity independent of carbonate lithofacies.
- Image analysis accurately quantifies total porosity in lithofacies that lack significant quantities of matrix pore types, however, in matrix pore dominated lithofacies (i.e. greater than 5 % total porosity composed of matrix pore types), total porosity is underestimated by 10 % or greater total porosity using the same image analysis

workflow. The underestimation of total porosity in matrix pore dominated lithofacies is thought to be caused by the incomplete imaging of micro porosity and non-representative field of views.

- Image analysis can be accurately used to quantify total porosity in porous lithofacies that lack or are weakly microporous, but not in microporous lithofacies. This suggests that image analysis can be reliably used to quantify pore system characteristics, such as size and shape, in weakly or non-microporous lithofacies, but not in microporous lithofacies.

Acknowledgements

The authors would like to thank Total E&P and BG Group for project funding and support and the Industry Technology Facilitator for enabling the collaborative development (grant number 3322PSD). The authors would also like to thank Aberdeen Formation Evaluation Society and the College of Physical Sciences at the University of Aberdeen for partial financial support. Dougal Jerram, Raymi Castilla, Claude Gout, Frances Abbots and an anonymous reviewer are thanked for their constructive comments and suggestions to improve the standard of this manuscript. The authors would also like to express their gratitude toJohn Still and Colin Taylor for technical assistance in the laboratory and Nick Timms (Curtin University) and Angela Halfpenny (CSIRO) for their assistance with the full thin section scanning equipment.

References

Andriani, G.., Walsh, N., 2002. Physical properties and textural parameters of calcarenitic rocks: qualitative and quantitative evaluations. Eng. Geol. 67, 5–15. doi:10.1016/S0013-7952(02)00106-0

Anselmetti, F.S., Luthi, S., Eberli, G.P., 1998. Quantitative Characterization of Carbonate Pore Systems by Digital Image Analysis. Am. Assoc. Pet. Geol. Bull. 82, 1815–1836.

Berrezueta, E., González-Menéndez, L., Ordóñez-Casado, B., Olaya, P., 2015. Pore network quantification of sandstones under experimental CO2 injection using image analysis. Comput. Geosci. 77, 97–110. doi:10.1016/j.cageo.2015.01.005

Cantrell, D.L., Hagerty, R.M., 1999. Microporosity in Arab formation carbonates: Saudi Arabia. GeoArabia 4, 129–154.

Cerepi, A., Humbert, L., Burlot, R., 2001. Petrophysical properties of porous medium from Petrographic Image Analysis data. Colloids Surfaces A Physiochemical Enginering Asp. 187-188, 233–256.

Choquette, P.W., Pray, L.C., 1970. Geologic Nomenclature and Classification of Porosity in Sedimentary Carbonates. Am. Assoc. Pet. Geol. Bull. 54, 207–250.

Deville de Periere, M., Durlet, C., Vennin, E., Lambert, L., Bourillot, R., Caline, B., Poli, E., 2011. Morphometry of micrite particles in cretaceous microporous limestones of the Middle East: Influence on reservoir properties. Mar. Pet. Geol. 28, 1727–1750.

Ehrlich, R., Crabtree, S.J., Horkowitz, K.O., Horkowitz, J.P., 1991. Petrography and Reservoir Physics 1: Objective Classification of Reservoir Porosity. Am. Assoc. Pet. Geol. Bull. 75, 1547–1562.

Galaup, S., Liu, Y., Cerepi, A., 2012. New integrated 2D–3D physical method to evaluate the porosity and microstructure of carbonate and dolomite porous system. Microporous Mesoporous Mater. 154, 175–186. doi:10.1016/j.micromeso.2011.12.021

Grove, C., Jerram, D.A., 2011. jPOR: An ImageJ macro to quantify total optical porosity from blue-stained thin sections. Comput. Geosci. 37, 1850–1859.

Halley, R.B., 1978. Estimating pore and cement volumes in thin section. J. Sediment. Res. 48, 642–650.

Healy, D., Neilson, J.E., Haines, T.J., Michie, E.A.H., Timms, N.E., Wilson, M.J., 2014. An investigation of porosity-velocity relationships in faulted carbonates using outcrop analogues. Geol. Soc. London, Spec. Publ. 406. doi:10.1144/SP406.13

Hollis, C., Vahrenkamp, V., Tull, S., Mookerjee, A., Taberner, C., Huang, Y., 2010. Pore system characterisation in heterogeneous carbonates: An alternative approach to widely-used rock-typing methodologies. Mar. Pet. Geol. 27, 772–793.

Jerram, D.A., Higgins, M.D., 2007. 3D Analysis of Rock Textures: Quantifying Igneous Microstructures. Elements 3, 239–245. doi:10.2113/gselements.3.4.239

Lønøy, A., 2006. Making sense of carbonate pore systems. Am. Assoc. Pet. Geol. Bull. 90, 1381–1405.

Michie, E.A.H., Haines, T.J., Healy, D., Neilson, J.E., Timms, N.E., Wibberley, C.A.J., 2014. Influence of carbonate facies on fault zone architecture. J. Struct. Geol. 65, 82–99. doi:10.1016/j.jsg.2014.04.007

Mock, A., Jerram, D.A., 2005. Crystal size distributions (CSD) in three dimensions: Insights from the 3D reconstruction of a highly porphyritic rhyolite. J. Petrol. 46, 1525–1541. doi:10.1093/petrology/egi024

Morgan, D.J., Jerram, D.A., 2006. On estimating crystal shape for crystal size distribution analysis. J. Volcanol. Geotherm. Res. 154, 1–7. doi:10.1016/j.jvolgeores.2005.09.016

Mowers, T.T., Budd, D.A., 1996. Quantification of Porosity and Permeability Reduction Due to Calcite Cementation Using Computer-Assisted Petrographic Image Analysis Techniques. Am. Assoc. Pet. Geol. Bull. 80, 309–322.

Neto, I.A.L., Misságia, R.M., Ceia, M.A., Archilha, N.L., Oliveira, L.C., 2014. Carbonate pore system evaluation using the velocity – porosity – pressure relationship, digital image analysis, and differential effective medium theory. J. Appl. Geophys. 110, 23–33. doi:10.1016/j.jappgeo.2014.08.013

Pedley, H.M., 1978. A new lithostratigraphical and palaeoenvironmental interpretation for the coralline limestone formations of the Maltese Islands (Miocene). Overseas Geol. Miner. Resour. 54, 273–291.

Pedley, H.M., House, M.R., Waugh, B., 1976. The geology of Malta and Gozo. Proc. Geol. Assoc. 87, 325–341.

Rasband, W.S., 2014. ImageJ. http://imagej.nih.gov/ij/.

Rustichelli, A., Tondi, E., Agosta, F., Celma, C. Di, Giorgioni, M., 2013. Sedimentologic and diagenetic controls on pore-network characteristics of Oligocene - Miocene ramp carbonates (Majella Mountain, central Italy). Am. Assoc. Pet. Geol. Bull. 97, 487–524.

Solymar, M., Fabricius, I.L., 1999. Image analysis and estimation of porosity and permeability of Arnager Greensand, Upper Cretaceous, Denmark. Phys. Chem. Earth, Part A Solid Earth Geod. 24, 587–591.

Tucker, M., Graham, J., McManus, J., Miller, J., Harwood, G., Hardy, R., Trewin, N., Fairchild, I., Hendry, G., Quest, M., 1988. Techniques in Sedimentology.

Weger, R.J., Eberli, G.P., Baechle, G.T., Massaferro, J.L., Sun, Y.-F., 2009. Quantification of pore structure and its effect on sonic velocity and permeability in carbonates. Am. Assoc. Pet. Geol. Bull. 93, 1297–1317.

Wildenschild, D., Sheppard, A.P., 2013. X-ray imaging and analysis techniques for quantifying pore-scale structure and processes in subsurface porous medium systems. Adv. Water Resour. 51, 217–246. doi:10.1016/j.advwatres.2012.07.018

Zhang, X., Liu, B., Wang, J., Zhang, Z., Shi, K., Wu, S., 2014. Adobe photoshop quantification (PSQ) rather than point-counting: A rapid and precise method for quantifying rock textural data and porosities. Comput. Geosci. 69, 62–71. doi:10.1016/j.cageo.2014.04.003

Table Captions

Table 1 - Summary of the lithofacies classification of the Oligo-Miocene stratigraphy of the Maltese Islands.

Table 2 - Pore type compositions of the studied lithofacies units. Pore types are quoted as percentages of the total amount of macro and meso porosity, which is defined as pore greater than 10 µm in diameter or greater. The total amount of macro and meso porosity calculated using image analysis.

Tables

Formation	Member	Lithofacies unit	Notation
Globigerina Limestone	Middle Globigerina Limestone	Planktonic Foraminifera Wackestones	PFW
	Lower Globigerina Limestone	Planktonic Foraminifera Wackestones	PFW
		Bryozoa Wackestones	BW
Lower Coralline Limestone	Il Mara	Reworked Bioclastic Packstones	RBP
	Xlendi	Coralline Algae Pack/ Grainstones	CAP/G
		Larger Benthic Foraminifera Pack/ Rudstones	LBFP/R
	Attard	Rhodolith Floatstones	RF

Table 1

Sample Number	*Formation* and Lithofacies	Macro + Meso porosity (He)	Pore types (% of optically visible porosity)							
			Inter-granular	Intra-granular	Inter-crystalline	Matrix	Mouldic	Vuggy	Fracture	Breccia
Globigerina Limestone										
12-43	PFW	*5.55*	*0.00*	*0.23*	*0.00*	*0.23*	*0.00*	*0.09*	*5.00*	*0.00*
12-48		*23.93*	*0.00*	*2.20*	*0.00*	*13.10*	*0.00*	*8.63*	*0.00*	*0.00*
12-49		*18.05*	*0.00*	*5.59*	*0.00*	*10.34*	*0.00*	*2.07*	*0.06*	*0.00*
12-50		*13.53*	*0.00*	*5.68*	*0.00*	*7.57*	*0.00*	*0.00*	*0.29*	*0.00*
12-58		*19.74*	*0.00*	*5.58*	*0.00*	*13.55*	*0.00*	*0.61*	*0.00*	*0.00*
12-59		*22.99*	*0.00*	*6.01*	*0.00*	*14.06*	*0.82*	*1.98*	*0.12*	*0.00*
12-64		*19.05*	*0.00*	*6.22*	*0.00*	*10.40*	*0.00*	*2.43*	*0.00*	*0.00*
12-87		*5.38*	*0.00*	*0.03*	*0.00*	*0.09*	*4.44*	*0.59*	*0.22*	*0.00*
12-93		*16.55*	*0.00*	*4.16*	*0.00*	*8.13*	*1.80*	*1.32*	*1.13*	*0.00*
12-94		*18.63*	*0.00*	*0.94*	*0.00*	*1.95*	*9.96*	*2.31*	*3.47*	*0.00*
12-95		*28.20*	*0.00*	*0.76*	*0.00*	*21.61*	*2.79*	*2.36*	*0.68*	*0.00*
12-96		*25.21*	*0.00*	*6.69*	*0.00*	*18.52*	*0.00*	*0.00*	*0.00*	*0.00*
12-182		*3.09*	*0.00*	*0.04*	*0.00*	*0.04*	*1.92*	*0.89*	*0.20*	*0.00*
12-67	BW	*13.88*	*0.00*	*11.43*	*0.00*	*1.89*	*0.00*	*0.46*	*0.11*	*0.00*
12-81		*18.00*	*0.00*	*15.04*	*0.00*	*2.09*	*0.12*	*0.29*	*0.46*	*0.00*
Lower Coralline Limestone										
12-42	RBP	*2.21*	*0.00*	*0.24*	*0.00*	*0.01*	*0.44*	*0.76*	*0.62*	*0.14*
12-44		*10.73*	*0.19*	*1.24*	*0.00*	*1.08*	*0.12*	*8.10*	*0.00*	*0.00*
12-45		*6.93*	*0.03*	*0.63*	*0.00*	*0.69*	*0.09*	*5.49*	*0.00*	*0.00*
12-53		*7.42*	*0.28*	*0.98*	*0.00*	*0.96*	*1.75*	*3.35*	*0.09*	*0.00*
12-54		*6.62*	*0.05*	*0.18*	*0.00*	*0.83*	*1.59*	*3.81*	*0.16*	*0.00*
12-68		*16.87*	*0.30*	*0.19*	*0.00*	*6.51*	*0.22*	*9.66*	*0.00*	*0.00*
12-77		*18.59*	*0.21*	*0.00*	*0.00*	*2.58*	*0.41*	*15.03*	*0.36*	*0.00*

12-88		*7.39*	*0.00*	*0.00*	*0.00*	*0.52*	*0.55*	*5.57*	*0.75*	*0.00*
12-89		*10.70*	*0.00*	*0.06*	*0.00*	*0.06*	*1.65*	*8.05*	*0.87*	*0.00*
12-86		*1.68*	*0.03*	*0.10*	*0.00*	*0.07*	*0.10*	*1.08*	*0.30*	*0.00*
12-91	CAP/G	*14.73*	*0.00*	*0.13*	*0.00*	*1.39*	*1.09*	*11.66*	*0.46*	*0.00*
12-92		*19.91*	*1.01*	*0.00*	*0.00*	*3.14*	*0.20*	*15.26*	*0.30*	*0.00*
12-157		*28.26*	*13.95*	*0.31*	*0.00*	*10.30*	*0.21*	*2.78*	*0.72*	*0.00*
12-159		*21.35*	*2.75*	*0.17*	*0.00*	*15.68*	*0.72*	*1.93*	*0.11*	*0.00*

Table 2

Figure Captions

Figure 1 - Optical photomicrographs (PPL) of carbonate lithofacies units used in the Oligo-Miocene stratigraphy of the Maltese Islands. A) Coralline algae packstone (CAP/G). B) Reworked bioclastic packstone (RBP). C) Bryozoa wackestone (BW). D) Planktonic foraminifera wackestone (PFW).

Figure 2 - Optical (PPL) and BSE-SEM photomicrographs of the same pore system highlighting the difference in porosity definition according to the type of photomicrograph. A) Full thin section optical photomicrograph of the Reworked Bioclastic Packstone (RBP) lithofacies, displaying the field of view in B and C. B) Optical photomicrograph of a pore system in which blue dyed epoxy resin has incompletely filled the porosity and therefore poorly defines the pore system. C) The same field of view in B under BSE-SEM conditions. The BSE-SEM image defines the pore system well.

Figure 3 - Image acquisition workflow employed in this study. A) Optical photomicrograph (PPL) of an x-thin section of the Planktonic Foraminifera Wackestone (PFW) lithofacies (Middle Globigerina Limestone Member). 6 BSE-SEM images were acquired from 3 locations on each thin section: at the bottom (B), centre (C) and top (T). B) 6 BSE-SEM photomicrographs acquired from the top (T) of the x-thin section. The fields of view in each of the 6 photomicrographs overlap; the 6 photomicrographs were stitched together to create a pore system image. C) A pore system image taken from the top (T) of the x-thin section.

Figure 4 - Image processing workflow employed in this study. BSE-SEM pore system images acquired from A) the x-thin section, B) the y-thin section and C) the z-thin section were combined to provide a 3D representation of the pore system, which is shown in D. E) The pore system images were systematically thresholded to create binary images (white = rock

phase, black = pore phase). The binary images were then inputted into image analysis software (ImageJ 1.48i) to quantify pore system characteristics.

Figure 5 - Impact of BSE-SEM pore system image magnification on the porosity values quantified by image analysis. Image analysis porosity has been quantified from the same field of view at five different magnifications. The magnification of the field of view increases from 47 x, in pore system image I, to 470 x, in pore system image V; this equates to a change in resolution from 3.151 to 0.032 μm^2 per pixel. The graph displays the change in image analysis porosity according to the increase in magnification of the pore system images.

Figure 6 - Impact of thin section sample area on porosity quantification in A) the PFW lithofacies and B) the RBP lithofacies. Inset: BSE-SEM photomicrographs of the two lithofacies. Average pore size is estimated using the Feret Diameter size descriptor.

Figure 7 - Histograms displaying total porosity quantified by A) He-porosimetry, B) mercury injection capillary pressure analysis and C) image analysis.

Figure 8 - Optical photomicrographs (PPL) displaying examples of the pore types in the studied lithofacies units (porosity = blue). A) Intergranular pores in the CAP/G lithofacies. B) Vuggy pores in the RBP lithofacies. C) Intragranular pores in the BW lithofacies. D) Matrix and intragranular pores in the PFW lithofacies.

Figure 9 - Graphs comparing the total porosity quantified by different methodologies in corresponding samples. A comparison of A) He-porosimetry and MICP quantified porosity and B) He-porosity and image analysis quantified porosity. Linear regression analysis has been conducted to quantify the relationship between the different porosity quantification methodologies. The coefficient of determination, R^2, is labeled on each graph to quantify the strength of the linear regression relationship. The solid lines, which are labeled 1:1, represent

the relationship where the porosity values derived from the different methodologies are equal, i.e. y = 1*x*.

Figure 10 - Mean difference between He-porosity and image analysis porosity ($\Delta\phi$) subdivided according to primary lithofacies (see Table 1 and Figure 1). Colour coding corresponds to stratigraphic Members (purple = Attard, blue = Xlendi, green = Il Mara, red = LGL and orange = MGL). LGL = Lower Globigerina Limestone Member and MGL = Middle Globigerina Limestone Member. The red line indicates that there is no difference between the He-porosity and the image analysis porosity.

Figure 11 - Mean porosity difference between He-porosity and image analysis porosity and the amount of porosity composed of matrix pore types. The solid line, which is labeled 1:1, represents the relationship where the mean porosity difference and the amount of porosity composed of different pore types is equal, i.e. y = 1*x*.

Figure 12 - Histograms comparing porosity distributions derived from helium porosimetry and image analysis in the RBP and BW lithofacies. In the RBP lithofacies: A) He-porosity and B) image analysis porosity. In the BW lithofacies: C) He-porosity and D) image analysis porosity. Insets: Optical photomicrographs of the corresponding lithofacies.

Figure 13 - Schematic cross section of a thin section in a micrite supported lithofacies showing the ‘hidden’ micro porosity hosted within the micritic matrix. This ‘hidden’ porosity is unlikely to be captured by image analysis techniques because the methodology images the top surface of the thin section; ‘hidden’ porosity is therefore considered to be one of the key causes of the underestimation of image analysis porosity in this study.

680 # Figures

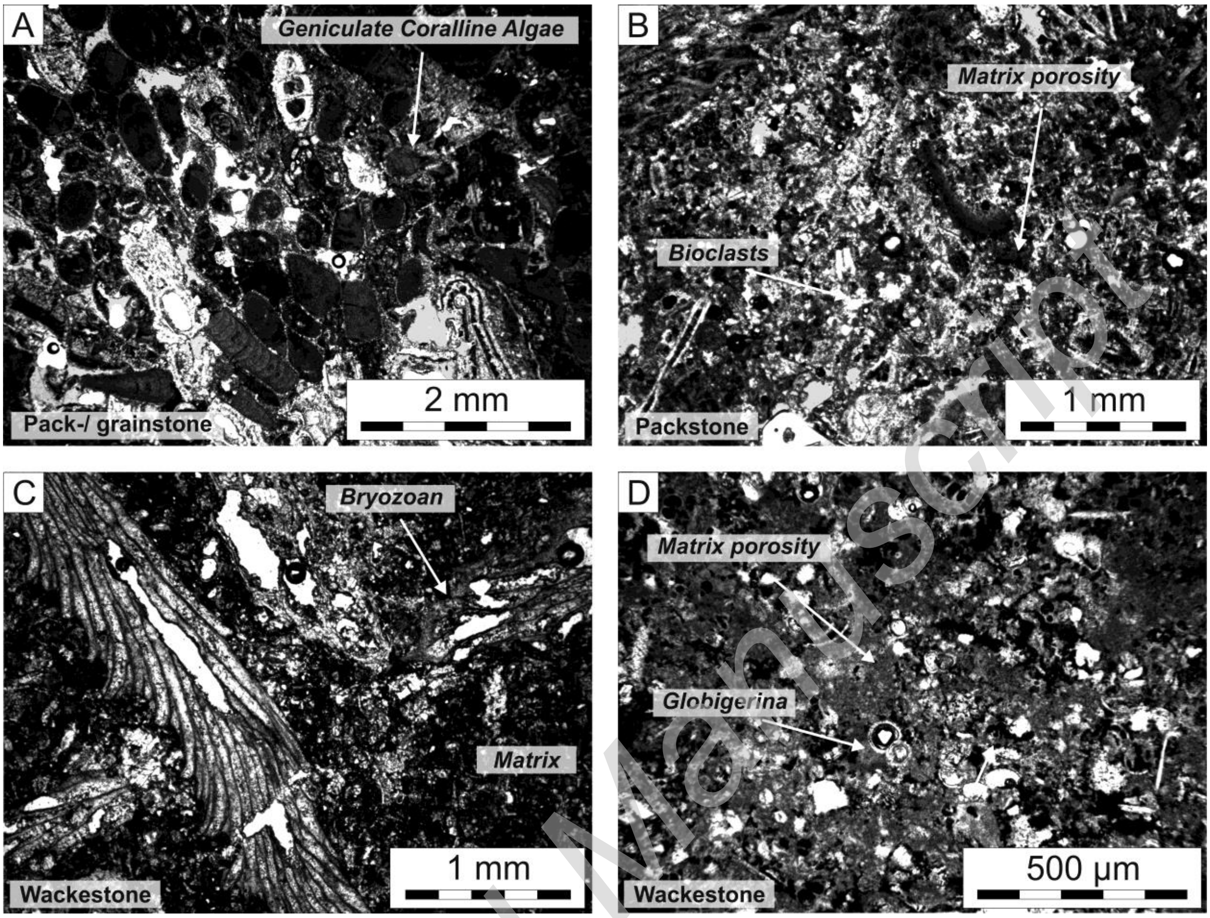

681

682 Figure 1

683

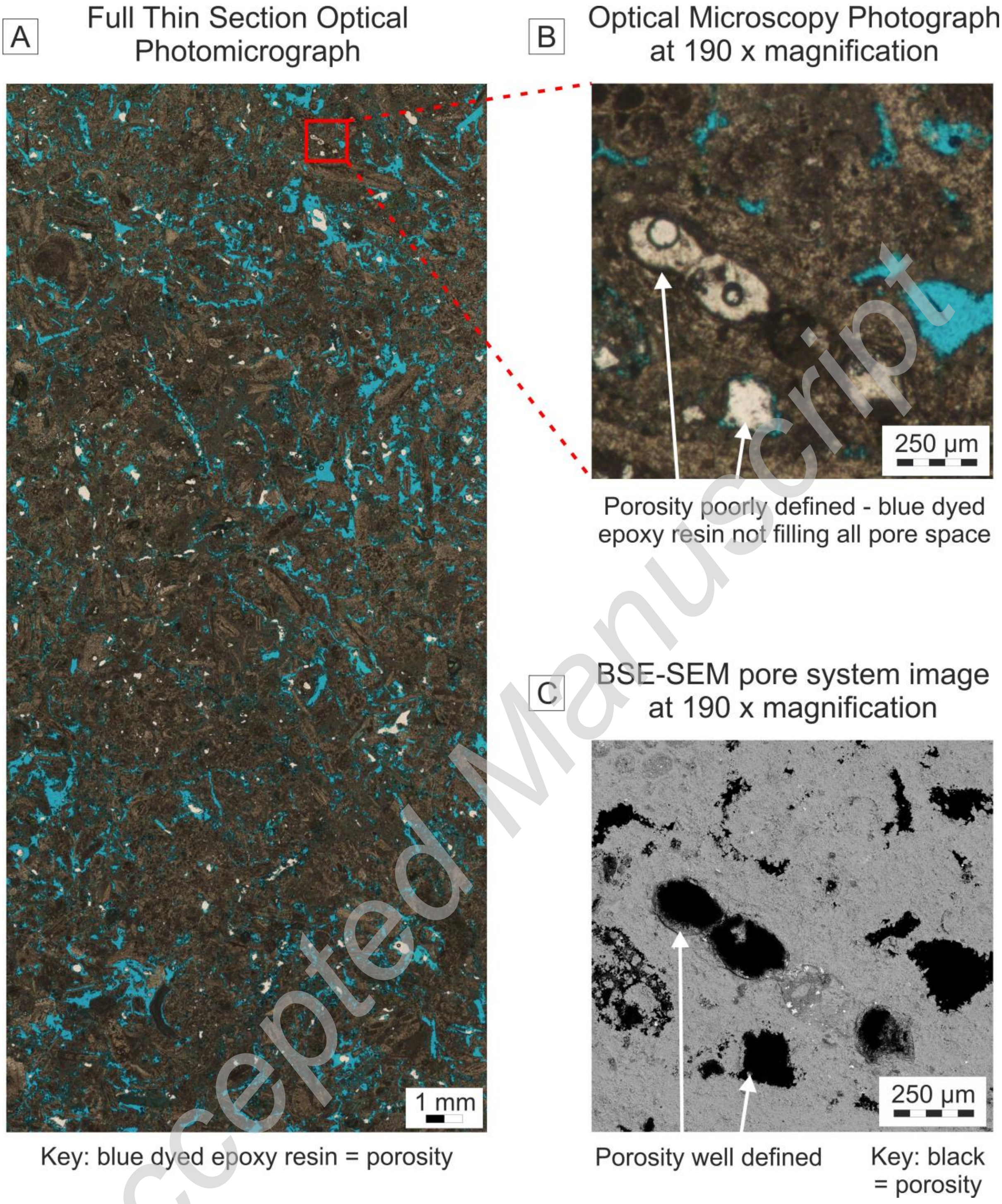

684

685 Figure 2

686

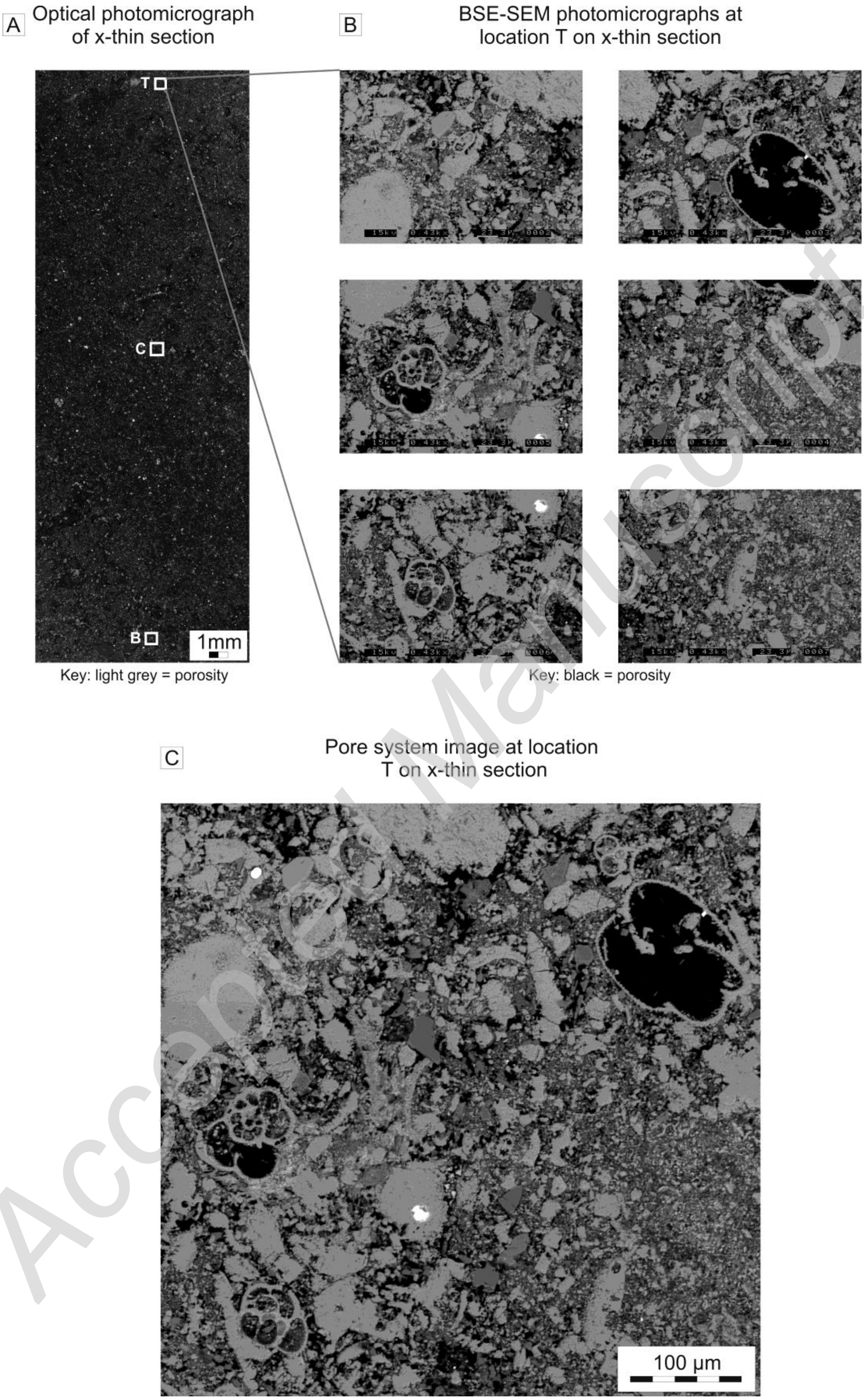
A
Optical photomicrograph of x-thin section
B
BSE-SEM photomicrographs at location T on x-thin section
T
C
B
1mm
Key: light grey = porosity
Key: black = porosity
C
Pore system image at location T on x-thin section
100 μm

Figure 3

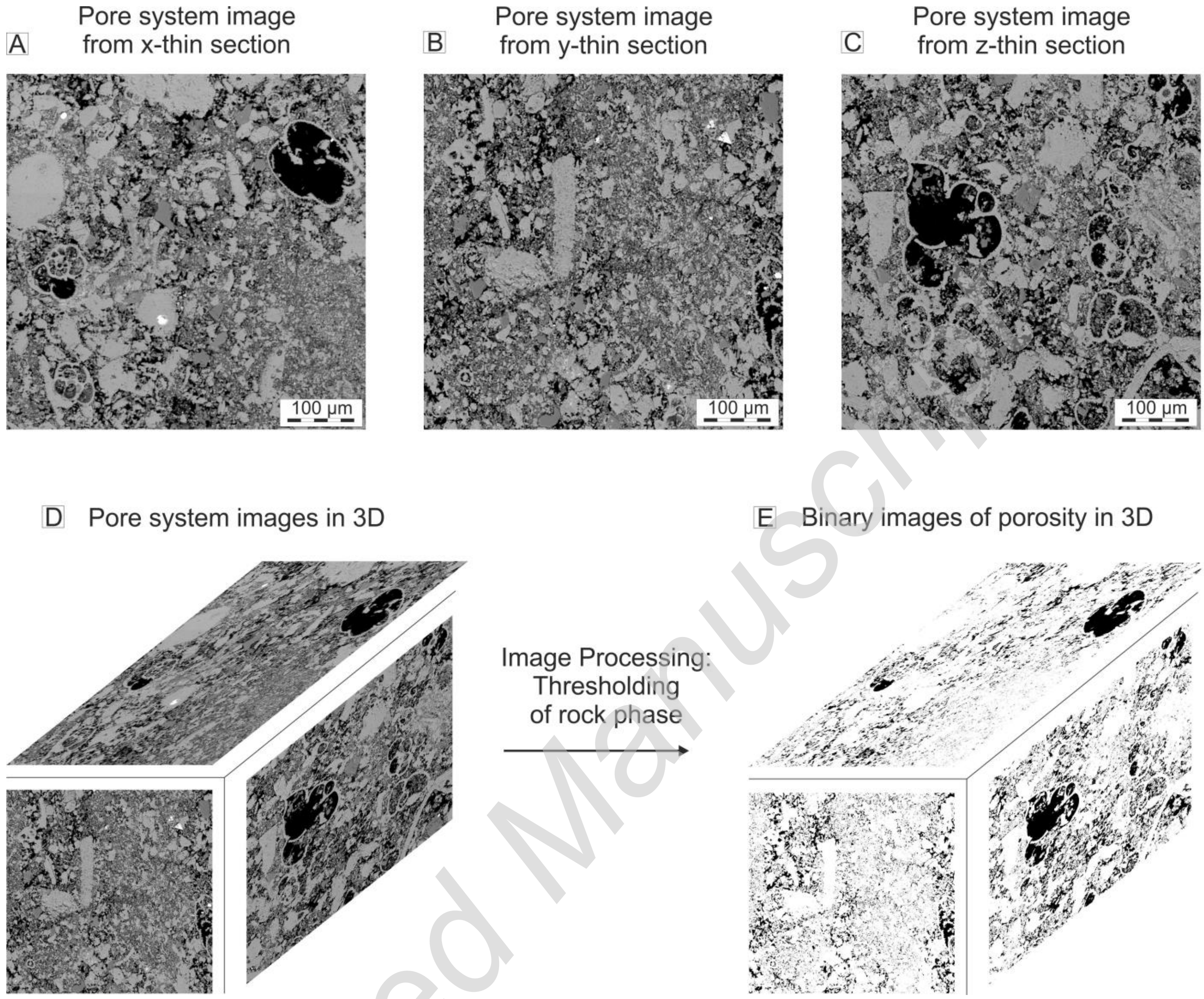
A
Pore system image from x-thin section
B
Pore system image from y-thin section
C
Pore system image from z-thin section
100 µm
100 µm
100 µm
D
Pore system images in 3D
Image Processing: Thresholding of rock phase
E
Binary images of porosity in 3D

Figure 4

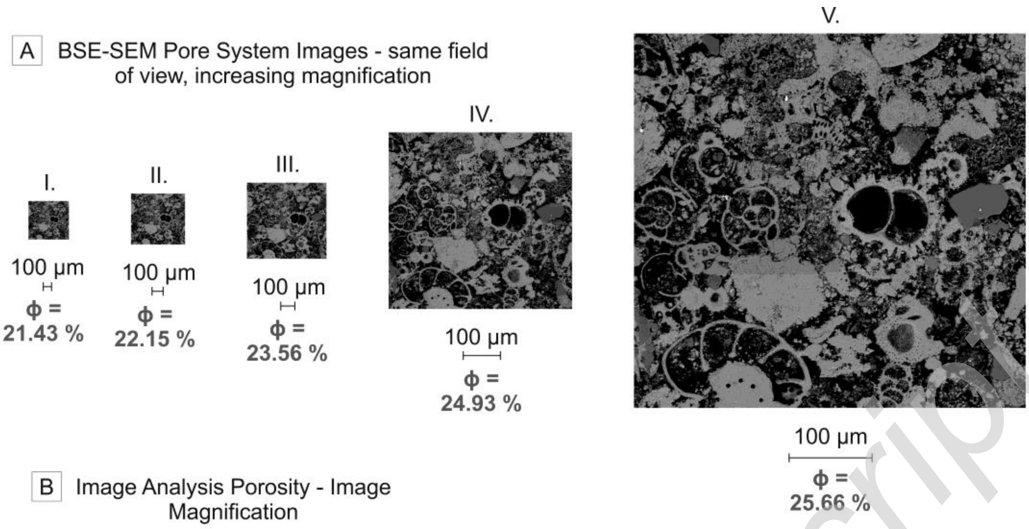

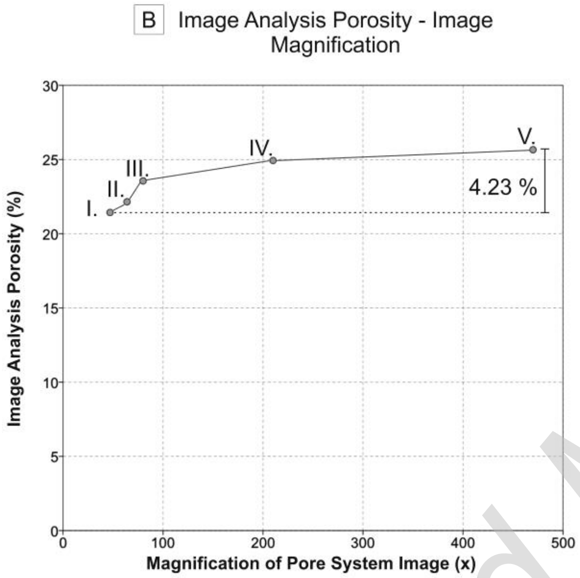

Photomicrograph	Magnification (x)	Pixel Resolution (μm^2/ pixel)
I	47	3.151
II	64	1.756
III	80	1.085
IV	210	0.157
V	470	0.032

Figure 5

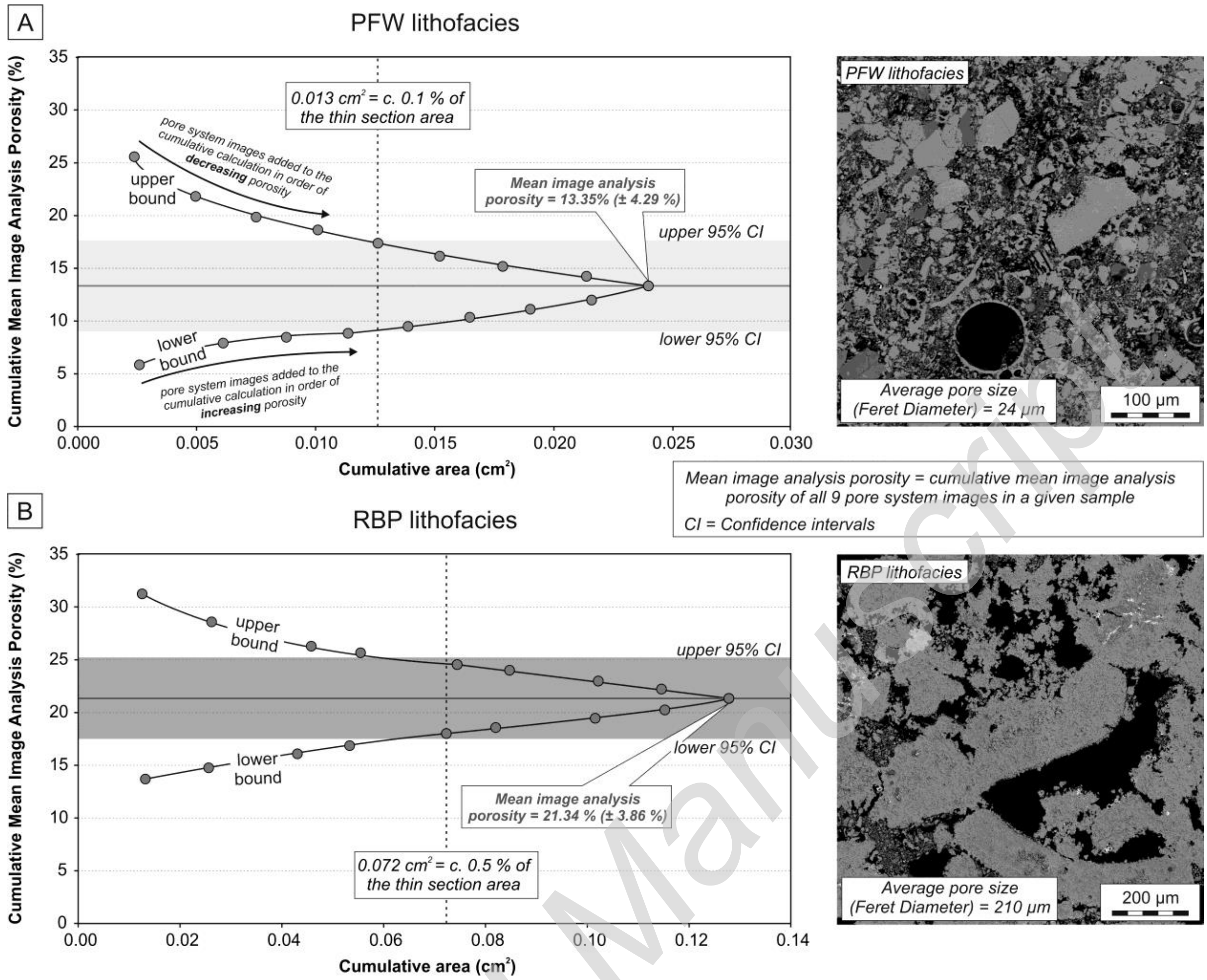

694

695 Figure 6

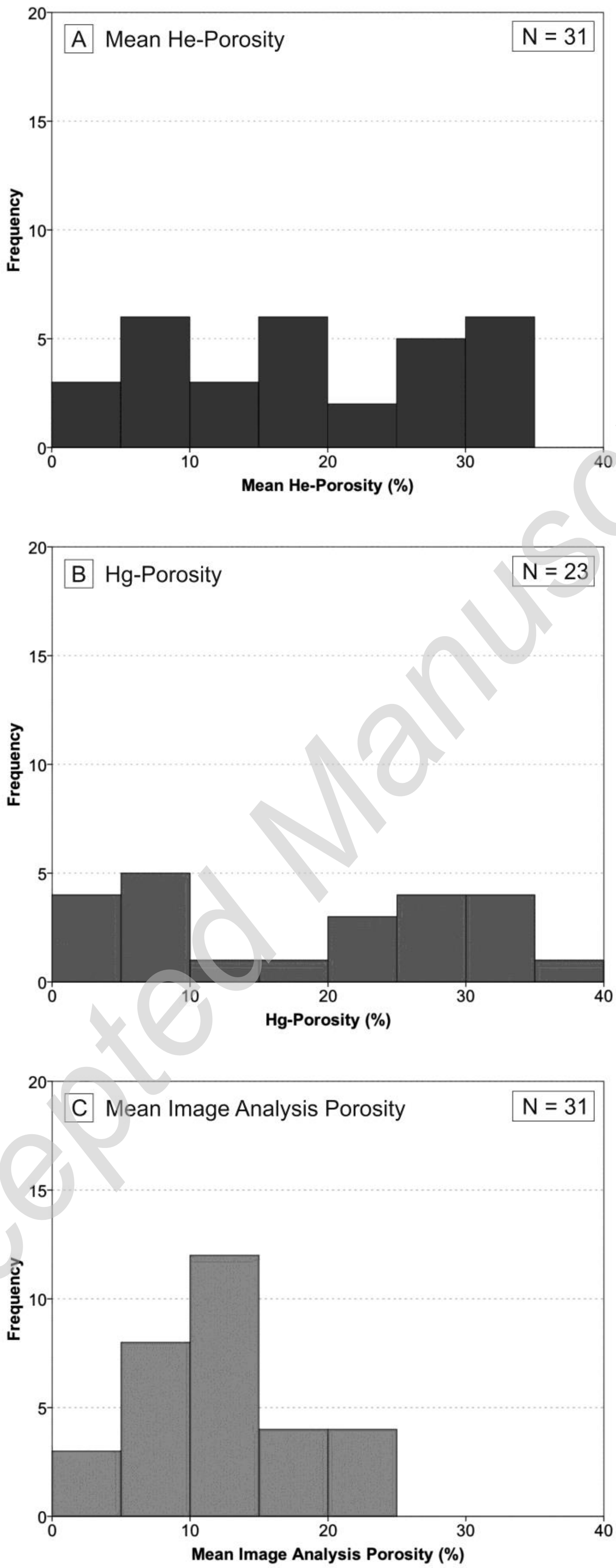

696

697 Figure 7

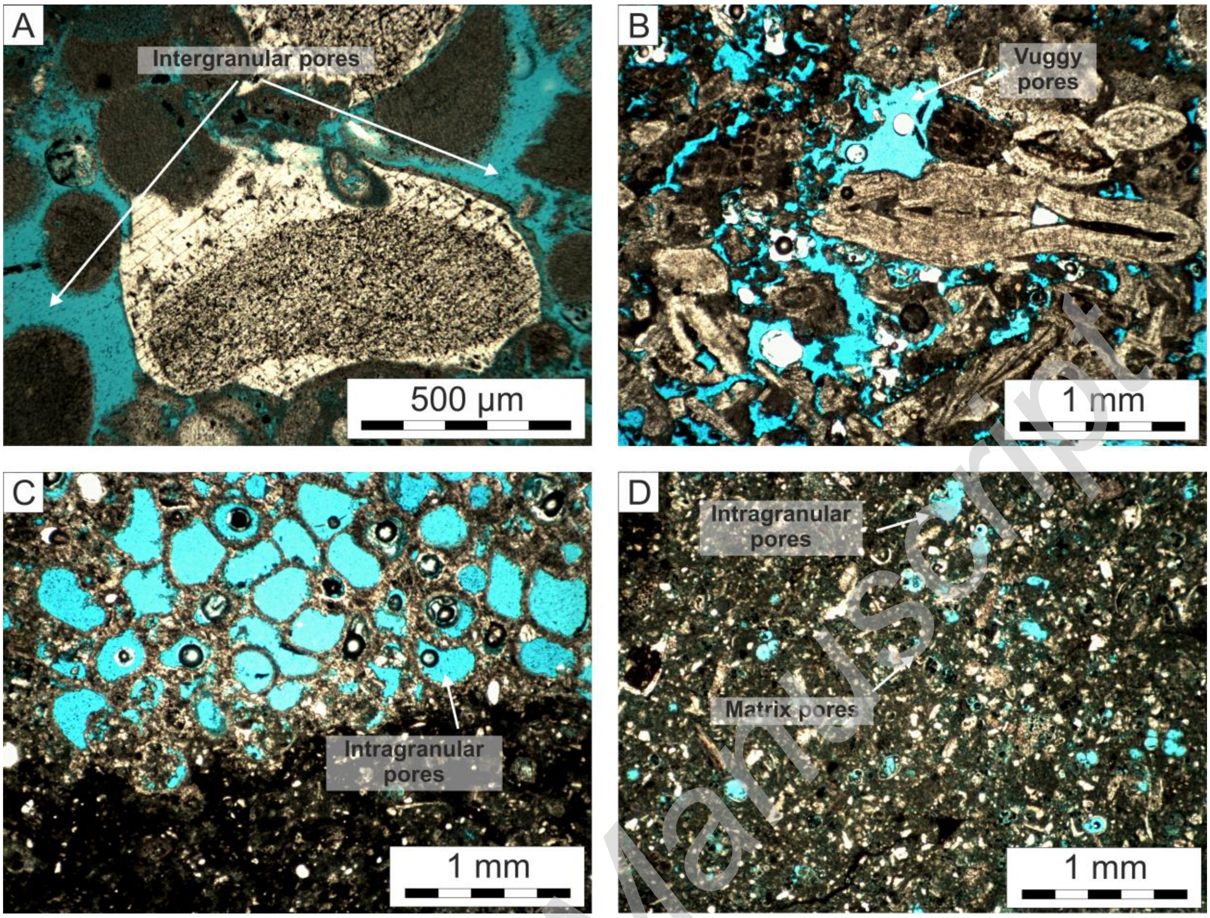
A
Intergranular pores
500 µm
B
Vuggy pores
1 mm
C
Intragranular pores
1 mm
D
Intragranular pores
Matrix pores
1 mm

Figure 8

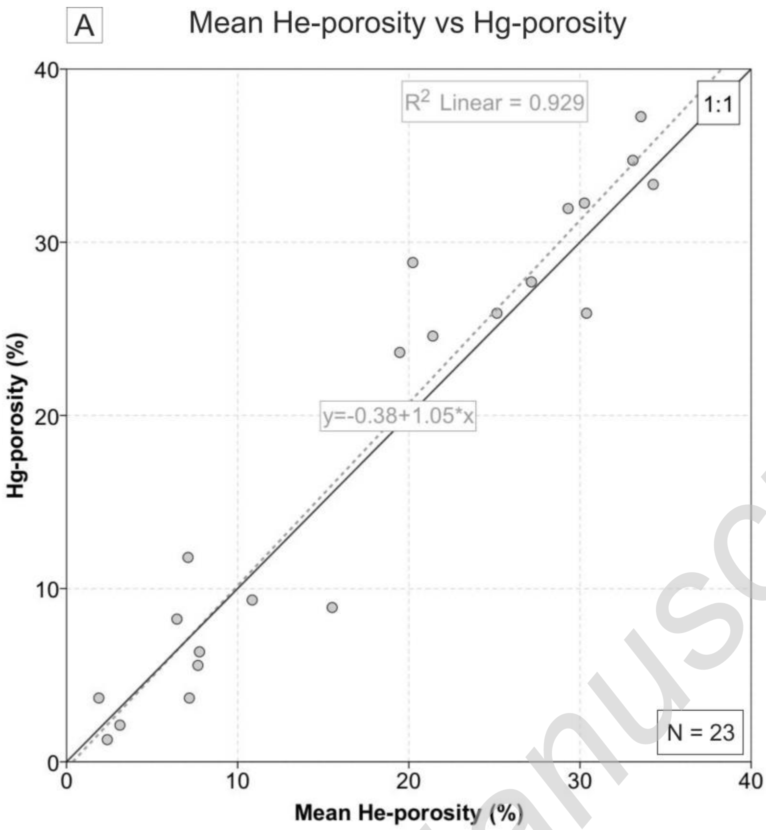
A
Mean He-porosity vs Hg-porosity
R2 Linear = 0.929
1:1
y=-0.38+1.05*x
N = 23
Hg-porosity (%)
Mean He-porosity (%)
0
10
20
30
40

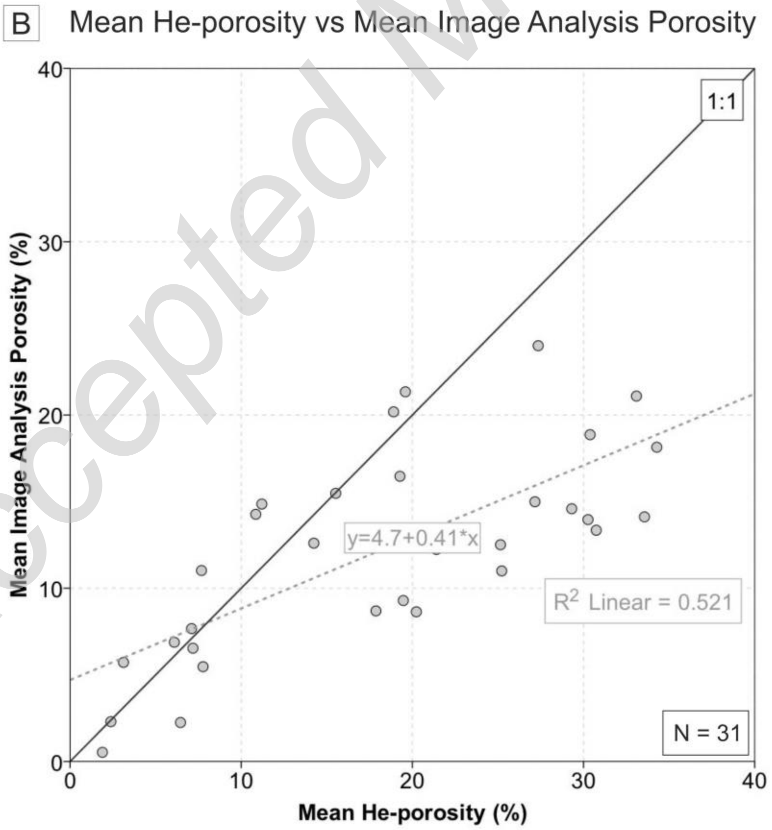
B
Mean He-porosity vs Mean Image Analysis Porosity
1:1
y=4.7+0.41*x
R2 Linear = 0.521
N = 31
Mean Image Analysis Porosity (%)
Mean He-porosity (%)
0
10
20
30
40

Figure 9

703

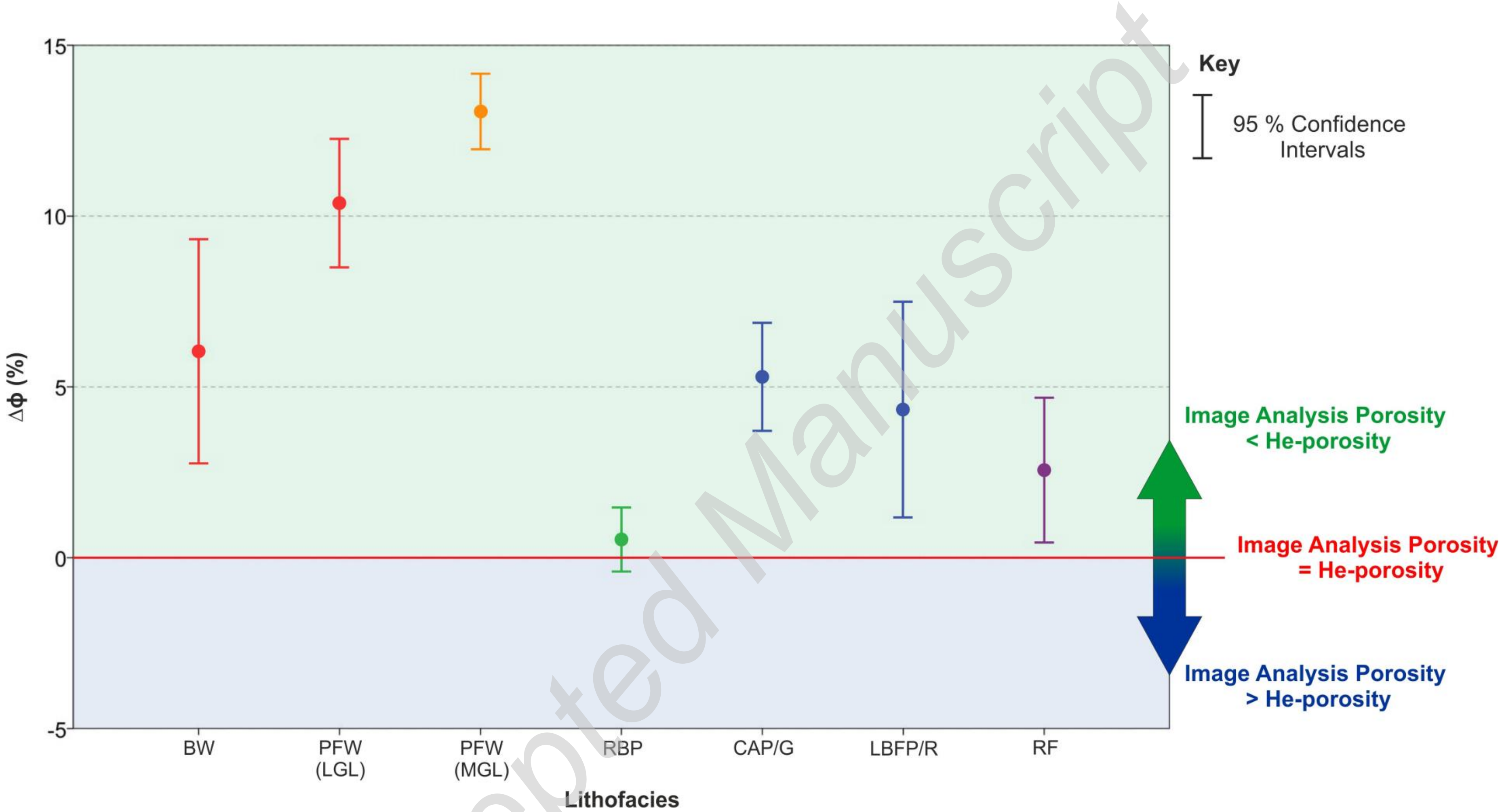

704 Figure 10

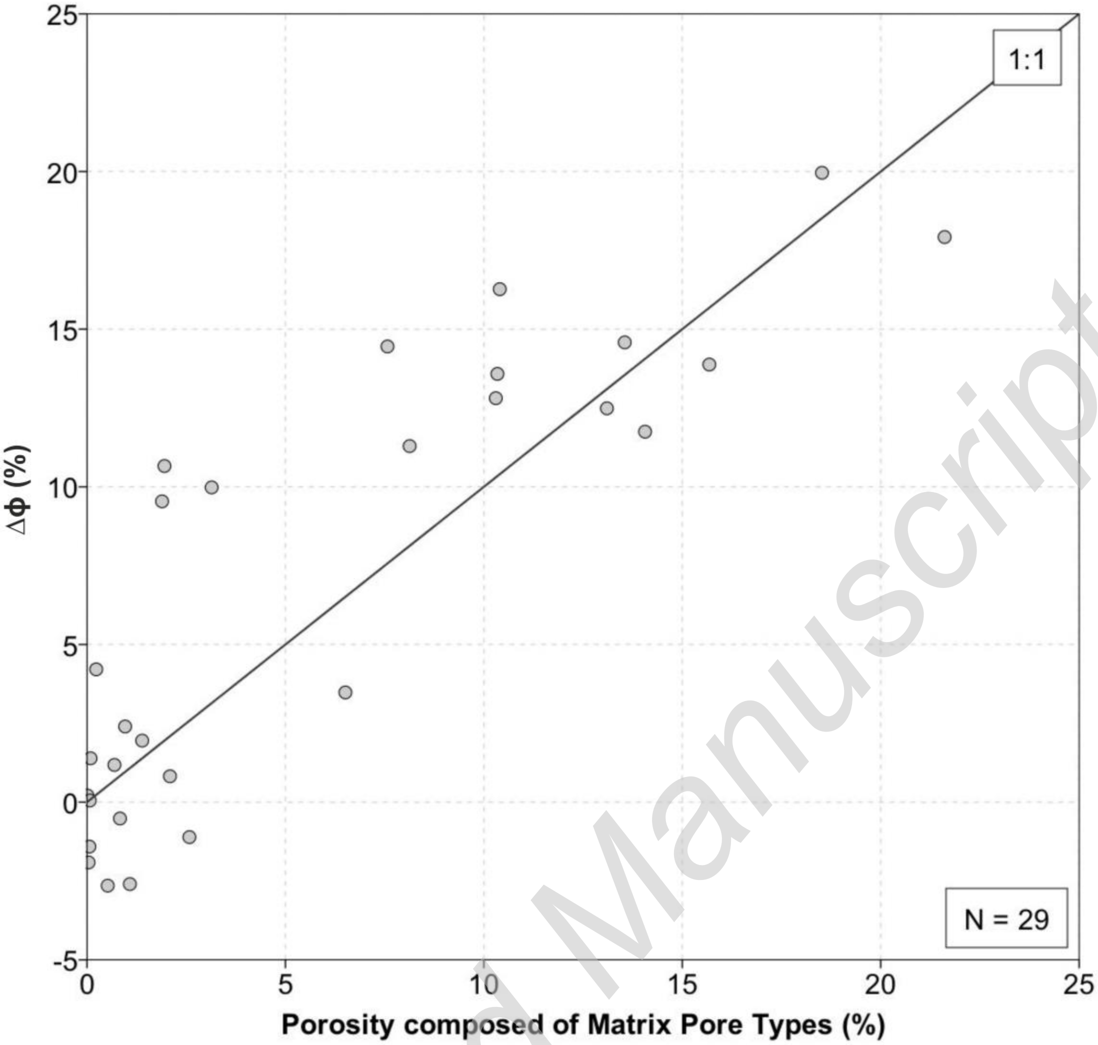

1:1
N = 29
Δϕ (%)
Porosity composed of Matrix Pore Types (%)
-5
0
5
10
15
20
25

Figure 11

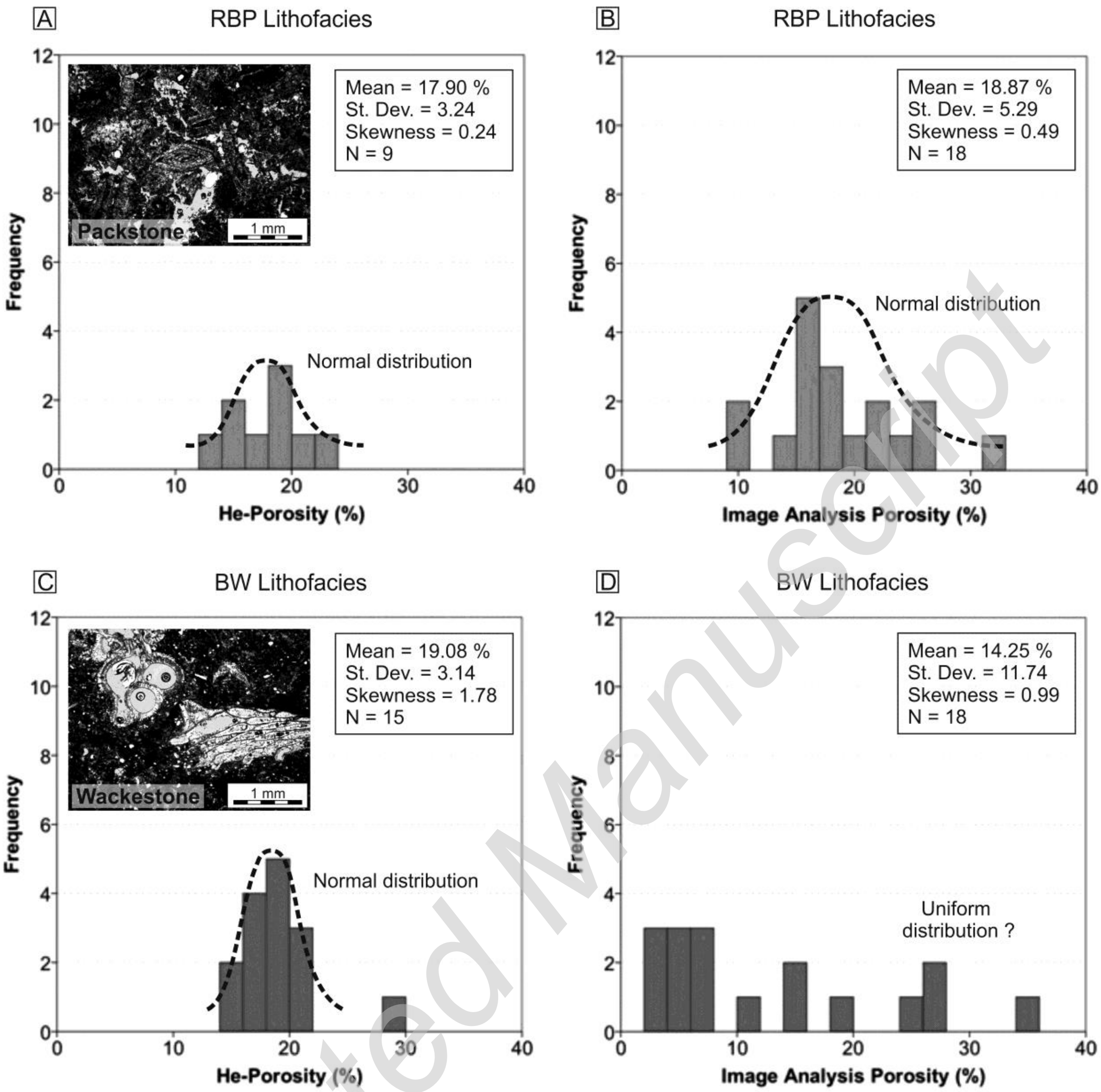
A
RBP Lithofacies
Packstone
1 mm
Mean = 17.90 %
St. Dev. = 3.24
Skewness = 0.24
N = 9
Normal distribution
Frequency
He-Porosity (%)
B
RBP Lithofacies
Mean = 18.87 %
St. Dev. = 5.29
Skewness = 0.49
N = 18
Normal distribution
Frequency
Image Analysis Porosity (%)
C
BW Lithofacies
Wackestone
1 mm
Mean = 19.08 %
St. Dev. = 3.14
Skewness = 1.78
N = 15
Normal distribution
Frequency
He-Porosity (%)
D
BW Lithofacies
Mean = 14.25 %
St. Dev. = 11.74
Skewness = 0.99
N = 18
Uniform
distribution ?
Frequency
Image Analysis Porosity (%)

Figure 12

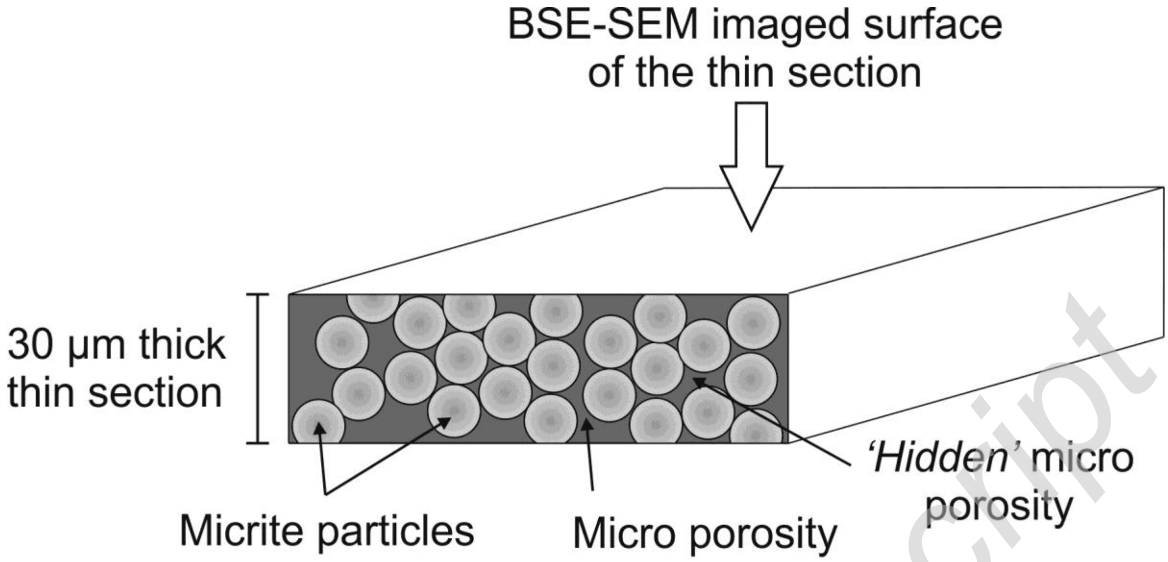
BSE-SEM imaged surface
of the thin section
30 µm thick
thin section
'Hidden' micro
porosity
Micrite particles
Micro porosity

Figure 13